

Article

## Structural and Affinity Analyses of G-Quadruplex DNA Aptamers for Camptothecin Derivatives

Hiroto Fujita<sup>1</sup>, Yuri Imaizumi<sup>1</sup>, Yuuya Kasahara<sup>1</sup>, Shunsuke Kitadume<sup>1</sup>, Hiroaki Ozaki<sup>1,2</sup>, Masayasu Kuwahara<sup>1,2,\*</sup> and Naoki Sugimoto<sup>3,4</sup>

<sup>1</sup> Graduate School of Science and Technology, Gunma University, 1-5-1 Tenjin-cho, Kiryu, Gunma 376-8515, Japan

<sup>2</sup> Division of Molecular Science, Faculty of Science and Technology, Gunma University, 1-5-1 Tenjin-cho, Kiryu, Gunma 376-8515, Japan

<sup>3</sup> Frontier Institute for Biomolecular Engineering Research (FIBER), Konan University, 7-1-20 Minatojima-minamimachi, Kobe 650-0047, Japan

<sup>4</sup> Faculty of Frontiers of Innovative Research in Science and Technology (FIRST), Konan University, 7-1-20 Minatojima-minamimachi, Kobe 650-0047, Japan

\* Author to whom correspondence should be addressed; E-Mail: mkuwa@gunma-u.ac.jp; Tel.: +81-277-30-1222; Fax: +81-277-30-1222.

Received: 1 July 2013; in revised form: 11 August 2013 / Accepted: 26 August 2013 /

Published: 29 August 2013

---

**Abstract:** We recently selected DNA aptamers that bind to camptothecin (CPT) and CPT derivatives from a 70-mer oligodeoxyribonucleotide (ODN) library using the Systematic Evolution of Ligands by EXponential enrichment (SELEX) method. The target-binding activity of the obtained 70-mer CPT-binding DNA aptamer, termed CA-70, which contains a 16-mer guanine (G)-core motif (G<sub>3</sub>TG<sub>3</sub>TG<sub>3</sub>T<sub>2</sub>G<sub>3</sub>) that forms a three-tiered G-quadruplex, was determined using fluorescence titration. In this study, truncated fragments of CA-70 that all have the G-core motif, CA-40, -20, -19, -18A, -18B, -17, and -16, were carefully analyzed. We found that CA-40 retained the target-binding activity, whereas CA-20, -19, and -18B exhibited little or no binding activities. Further, not only CA-18A but also the shorter length fragments CA-17 and -16 clearly retained the binding activity, indicating that tail strands of the G-quadruplex structure can significantly affect the target binding of G-quadruplex DNA aptamers. Further analyses using circular dichroism (CD) spectroscopy and fluorescence polarization (FP) assay were conducted to investigate the structure and affinity of G-quadruplex DNA aptamers.

**Keywords:** DNA aptamer; G-quadruplex; camptothecin (CPT); circular dichroism (CD) spectroscopy; fluorescence titration; fluorescence polarization (FP) assay

---

## 1. Introduction

Although nucleic acid aptamers with high binding affinity and specificity for various molecular targets have been created using SELEX methods [1–3], many of them, DNA aptamers in particular, are known to contain G-quadruplex structures [4–7]. Therefore, it is generally considered that DNA aptamers with G-quadruplexes can target a broad range of molecular structures while retaining specificity. In other words, the structural diversity of G-quadruplexes, *i.e.*, parallel; anti-parallel; and mixed parallel/anti-parallel strand configurations with loops and tails of various sequence combinations, can achieve specific recognition of many molecules, even those with a similar scaffold [8]. However, the roles of loops and tails in target–aptamer complex formation have not clearly been elucidated and remain a subject of investigation [9–12].

As mentioned above, we recently recovered CA-70 and observed an unexpected phenomenon in its affinity analyses using fluorescence titration [13]. Namely, CA-20, -19, and -18B exhibited little or no binding activities, whereas CA-18A, CA-17, and -16 clearly retained the binding activity. The experimental data urged us to conduct further experiments to investigate how tail strands of G-quadruplexes influence the target binding of aptamers. In addition, studying the effects of tail strands on the binding activity of G-quadruplex DNA aptamers for small molecules may be of great importance for researches of G-quadruplex formation in genomic DNA, because the clinical potential of G-quadruplex binding with small molecules in down regulating gene transcription has recently been demonstrated [14,15]. Thus, here we determined which nucleotide residues in tail strands are critical for CPT-binding of DNA aptamers and verified structural differences between active and inactive fragments.

## 2. Experimental Section

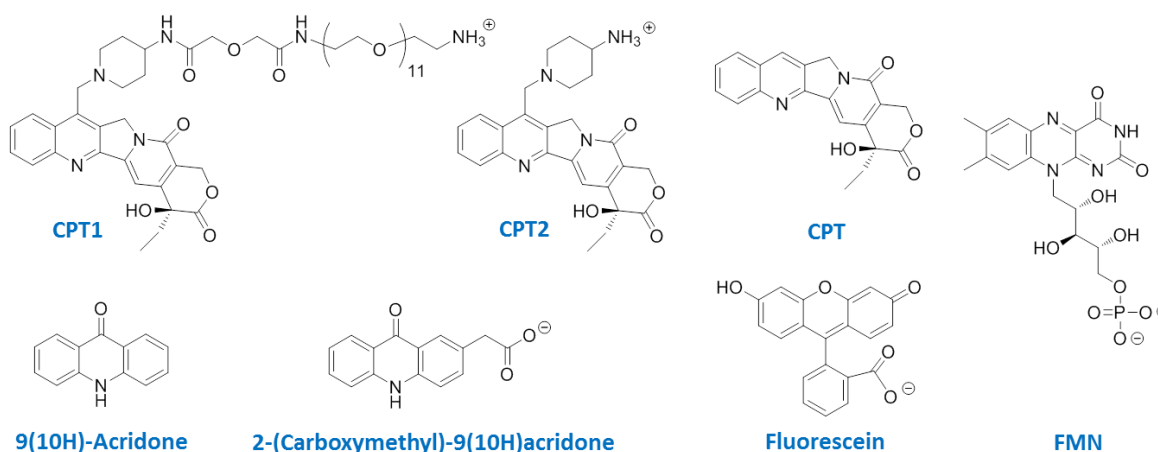
### 2.1. General

Ultraviolet-visible (UV-vis) spectra were measured using a U-3000 spectrophotometer (Hitachi High Technologies Corporation, Tokyo, Japan). Fluorescence spectra and fluorescence polarization were measured with a LS-55 spectrofluorophotometer (Perkin Elmer Japan Co., Ltd., Kanagawa, Japan). CD spectra were acquired with a JASCO J-820 spectrometer equipped with thermoelectrically controlled cell holders (JASCO Corporation, Tokyo, Japan). ODNs used were purchased from GeneDesign Inc. (Osaka, Japan) (Table 1). (*S*)-(+)-Camptothecin (CPT), 9(10*H*)-acridone, fluorescein, and polyoxyethylene sorbitan monolaurate (TWEEN<sup>®</sup> 20) were purchased from Tokyo Chemical Industry Co., Ltd. (Tokyo, Japan). Riboflavin-5'-phosphate sodium (FMN) was purchased from Yamasa Corporation (Chiba, Japan). The seven-substituted camptothecin derivatives (CPT1 and CPT2) were synthesized from CPT according to the method reported in the literature [13] (Figure 1). 2-(Carboxymethyl)-9(10*H*)acridone was synthesized according to the method reported in the literature [16].

**Table 1.** Sequences and binding affinities of CA-70 and its fragments.

Fragment	Sequence <sup>a</sup>							$K_d$ ( $\mu\text{M}$ ) <sup>b</sup>			
	Position	10	20	30	40	50	60	70	CPT1	CPT2	CPT
CA-70		GGTCAGCACGCTCCGGACTT	GGGTGGGTGGGT	TGGGGTACCGGTGCGTAATGTGTCGCTGAGCCTGCCAAC					1.8 ± 0.3	3.6 ± 0.2	4.6 ± 0.3
CA-40		ACGCTCCGGACTT	GGGTGGGTGGGT	TGGGGTACCGGTGCGT					3.0 ± 0.4	3.0 ± 0.2	5.6 ± 0.5
CA-23A		ACTT	GGGTGGGTGGGT	TGGGGTA					2.1 ± 0.9	n.d.	n.d.
CA-23B		TTTT	GGGTGGGTGGGT	TGGGGTA					>10	n.d.	n.d.
CA-20			TGGGTGGGTGGGT	TGGGGTA					>10	>10	>10
CA-19			GGGTGGGTGGGT	TGGGGTA					>10	>10	>10
CA-18A			TGGGTGGGTGGGT	TGGGG					6.0 ± 0.8	3.4 ± 0.3	>10
CA-18B			GGGTGGGTGGGT	TGGGGT					>10	>10	>10
CA-17			GGGTGGGTGGGT	TGGGG					8.1 ± 0.9	8.9 ± 1.0	>10
CA-16			GGGTGGGTGGGT	TGGGG					1.8 ± 0.3	2.7 ± 0.3	4.2 ± 0.4

<sup>a</sup> Sequences are aligned in the 5' to 3' direction. Regions of G-quadruplex motif are marked with yellow boxes. <sup>b</sup>  $K_d$  values were determined by fluorescence titration with the assumption that fragments bind targets in a 1:1 ratio. n.d., not determined.

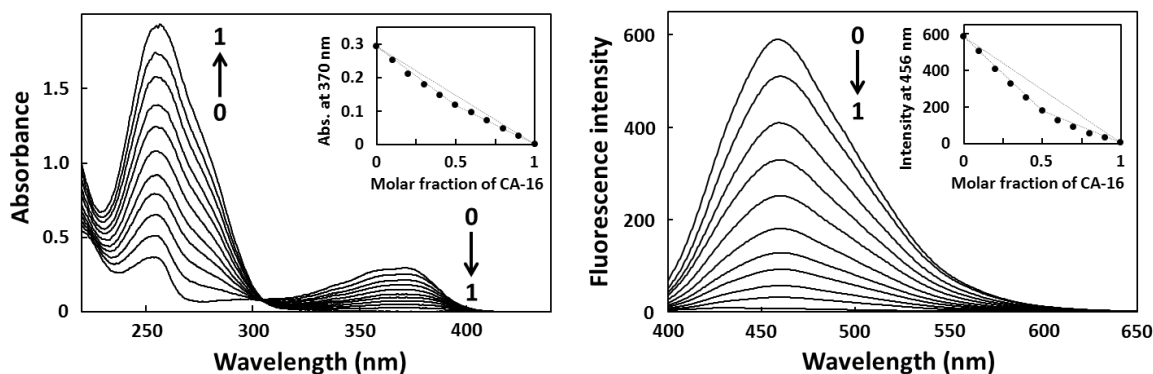
**Figure 1.** Chemical structures of analytes used in this study.

Buffer solutions were prepared using ultrapure water obtained using the Ultrapure Water system CPW-100 (Advantec Co. Ltd., Tokyo, Japan); 10 mM PBS buffer (pH 7.4) with 138 mM NaCl, 2.7 mM KCl, 2.5 mM MgCl<sub>2</sub>, and 0.05% TWEEN<sup>®</sup> 20, and 20 mM Tris-HCl buffer (pH 7.2) with different KCl concentrations (0, 5, 10, 20, and 50 mM).

## 2.2. Job Plot Analysis

To determine the binding stoichiometry between the aptamer and target, a continuous variation binding analysis (Job plot) was performed [17,18]. First, CA-16 was dissolved in 10 mM PBS buffer to make a final concentration of 10  $\mu\text{M}$ , and refolded by denaturing at 94 °C for 0.5 min, followed by cooling to 25 °C at a rate of 0.5 °C/min, while CPT1 was dissolved in 10 mM PBS buffer to make a final concentration of 10  $\mu\text{M}$ . These solutions were mixed to maintain the total molar concentration (CA-16 and CPT1) at 10  $\mu\text{M}$ , whereas the CA-16 mole fraction was varied at regular intervals from 0 to 1.0. After incubation at 25 °C for 30 min, the spectra of 11 sample solutions were measured using UV-vis spectroscopy and fluorescence spectroscopy to generate the Job plots (Figure 2).

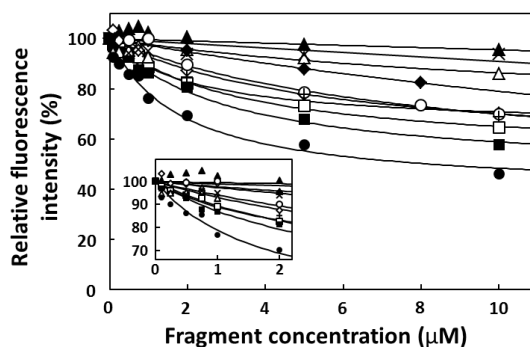
**Figure 2.** Continuous variation binding analysis (Job plot) of CPT1 using UV-vis spectroscopy (left) and fluorescence spectroscopy (right). Total concentration of CPT1 and CA-16 was maintained at 10  $\mu\text{M}$ .



### 2.3. Fluorescence Titration

Fluorescence titration of target (CPT1, CPT2, and CPT; final conc. 1.0  $\mu\text{M}$ ) with increasing concentrations of CA-70 and its fragments (final conc. 0–10  $\mu\text{M}$ ) was performed at 25  $^{\circ}\text{C}$  using LS-55. CA-70, -40, -23A, -23B, -20, -19, -18A, -18B, -17, and -16 were dissolved in 10 mM PBS buffer at appropriate concentrations (0–20  $\mu\text{M}$ ), and refolded by denaturing at 94  $^{\circ}\text{C}$  for 0.5 min and cooling to 25  $^{\circ}\text{C}$  at a rate of 0.5  $^{\circ}\text{C}/\text{min}$ . These solutions (50  $\mu\text{L}$  each) were mixed with 50  $\mu\text{L}$  solutions of target (CPT1, CPT2, and CPT; 2  $\mu\text{M}$ ) in 10 mM PBS buffer, respectively. Emission spectra of CPTs were obtained by exciting at 370 nm and monitoring fluorescence between 400 and 530 nm. In Figure 3, Y-axis indicates the relative fluorescence intensity (%) at 456 nm for CPT1 as an emission peak, where the intensity in the absence of fragments was set at 100%, and X-axis indicates fragment concentration. The relative fluorescence intensity (%) at 443 nm for CPT and at 456 nm for CPT2 was used to obtain the titration curves, respectively. The  $K_d$  values determined from the titration curves were listed on Table 1. To assess the binding specificity of CA-70, fluorescence titrations were also performed using the protocol described above and the following fluorophores: FMN, 9(10*H*)-acridone, 2-(carboxymethyl)-9(10*H*)acridone, and fluorescein (Figure 1).

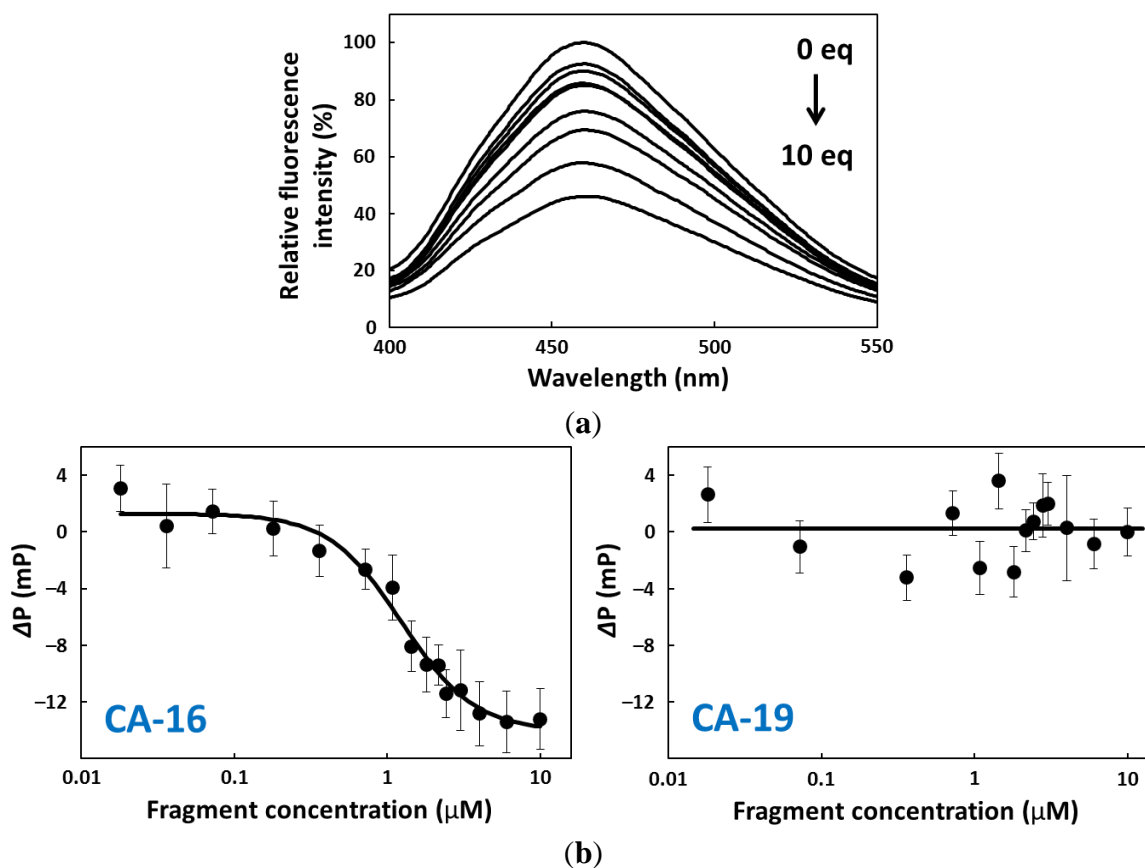
**Figure 3.** Titration curves for relative fluorescence intensity at 456 nm versus fragment concentration: CA-70 (open squares), CA-40 (closed squares), CA-23A (crosses), CA-23B (x-marks), CA-20 (open triangles), CA-19 (closed triangles), CA-18A (open diamonds), CA-18B (closed diamonds), CA-17 (open circles), and CA-16 (closed circles). CPT1 fluorescence without fragment was set at 100%.



## 2.4. FP Assay

Fluorescence polarization measurements were also made for CA-16 and -19 affinity analyses [19,20]. CA-16 and -19 were dissolved in 10 mM PBS buffer at appropriate concentrations (0–20  $\mu\text{M}$ ), and refolded by denaturing at 94  $^{\circ}\text{C}$  for 0.5 min and cooling to 25  $^{\circ}\text{C}$  at a rate of 0.5  $^{\circ}\text{C}/\text{min}$ . These solutions (50  $\mu\text{L}$  each) were mixed with 50  $\mu\text{L}$  solutions of CPT1 (2  $\mu\text{M}$ ) in 10 mM PBS buffer, respectively. Using LS-55, fluorescence polarizations for each of the mixtures described above were recorded every 20–30 seconds for 10 min with excitation at 372 nm and monitoring at 456 nm at 25  $^{\circ}\text{C}$ . These measurements were performed three times in independent experiments. Thus, fluorescence polarization results for CPT1 (final conc. 1.0  $\mu\text{M}$ ) at different fragment concentrations (final conc. 0–10  $\mu\text{M}$ ) were generated as shown in Figure 4b.

**Figure 4.** (a) Fluorescence spectra for CPT1 with varying CA-16 concentrations and excitation at 372 nm. CPT1 fluorescence without fragment was set at 100%. (b) Titration curve for CPT1 polarization versus fragment concentration: CA-16 (left) and CA-19 (right). Polarization was monitored at 456 nm using an excitation wavelength of 372 nm.  $\Delta P = P - P_0$ , where P is polarization with fragment, and  $P_0$  is polarization without fragment.

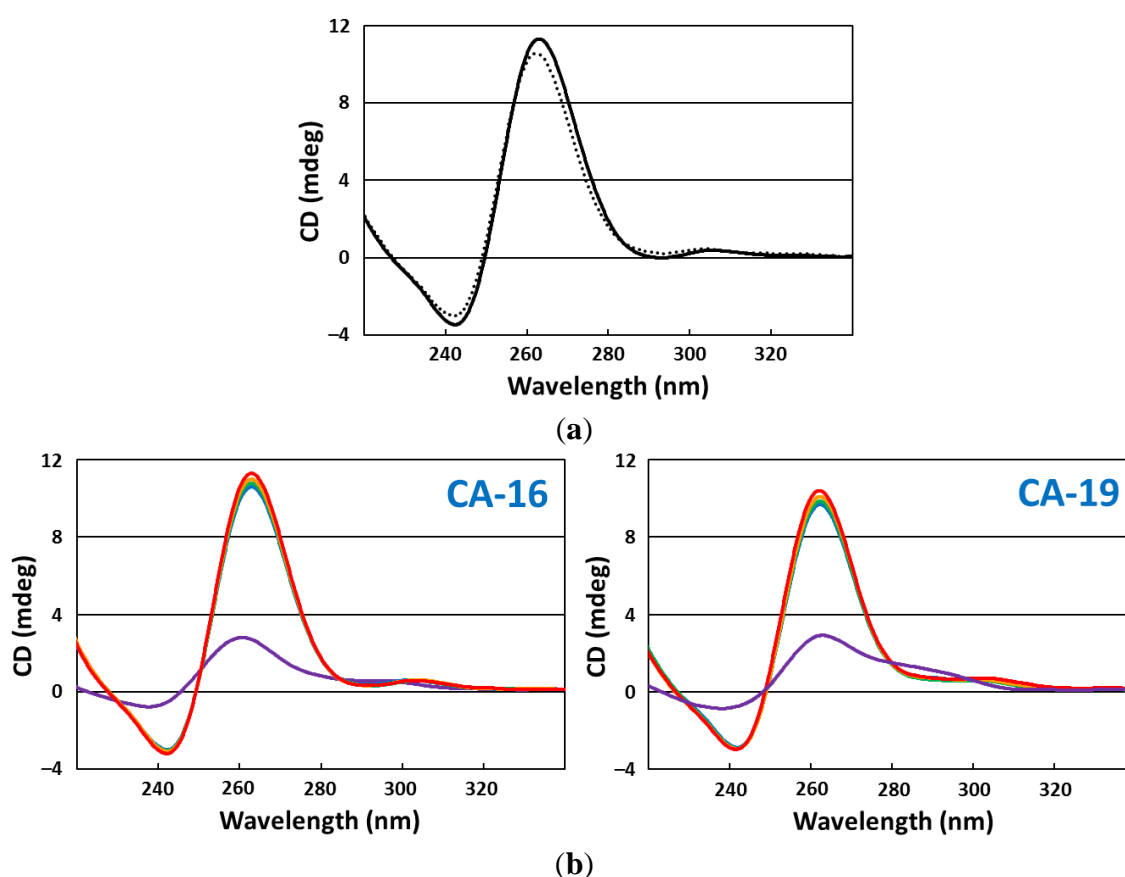


## 2.5. CD Spectroscopy

CD spectra were measured over a wavelength range of 220–340 nm using a quartz cuvette with a 1.0-mm optical path length. The scanning speed was set at 100 nm/min, and the response time was 1 s. Each spectrum was an average of five measurements made at 25  $^{\circ}\text{C}$ . Before CD measurements,

each fragment (CA-16 and -19) was dissolved in 20 mM Tris-HCl buffer (pH 7.2) for a 20  $\mu\text{M}$  solution followed by refolding by denaturing at 94  $^{\circ}\text{C}$  for 0.5 min and cooling to 25  $^{\circ}\text{C}$  at a rate of 0.5  $^{\circ}\text{C}/\text{min}$  using the thermal cycler. Sample solutions containing 10  $\mu\text{M}$  (final conc.) of fragment in 20 mM Tris-HCl buffer (pH 7.2) with different KCl concentrations (0, 5, 10, 20, and 50 mM) were prepared and analyzed (Figure 5). Similarly, the CD spectra of these fragments in 10 mM PBS buffer were measured.

**Figure 5.** CD spectra for (a) CA-16 (solid line) and CA-19 (dashed line) in 10 mM PBS buffer, pH 7.4, and for (b) CA-16 (left) and CA-19 (right) in 20 mM Tris-HCl buffer, pH 7.2, and with different  $\text{K}^+$  concentrations: 0 mM (purple), 5 mM (blue), 10 mM (green), 20 mM (orange), and 50 mM (red).



## 2.6. CD Melting Curves

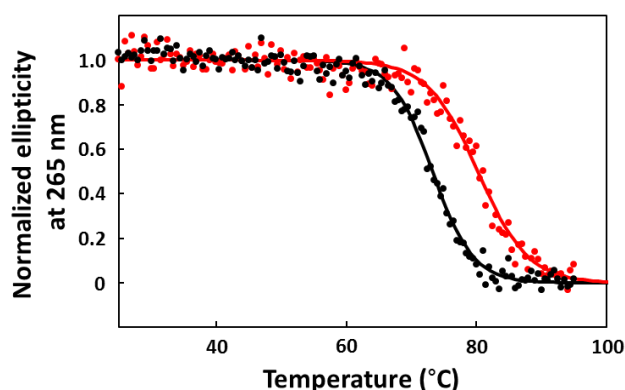
Ellipticity versus temperature profiles (melting curves) were measured at 265 nm in 0.1-cm path length cells. CA-16 was dissolved in 10 mM PBS buffer to make a final concentration of 10  $\mu\text{M}$ , and refolded as described above. Sample solutions of CA-16 with or without CPT1 (10  $\mu\text{M}$ ) were incubated at 25  $^{\circ}\text{C}$  for 30 min before CD measurements. Melting curve experiments were performed from 25  $^{\circ}\text{C}$  to 95  $^{\circ}\text{C}$  at a heating rate of 0.25  $^{\circ}\text{C}/\text{min}$ . The melting temperatures ( $T_m$ ), *i.e.*, the midpoint temperatures of the unfolding process, were determined on the basis of sigmoid curves produced by fitting the data points [21–23].



to CPT1 with a  $K_d$  value of 6.0  $\mu\text{M}$ , which was comparable to that of CA-17. Thus, these results indicate that the addition of a residue to CA-16 at the 3'-end but not at the 5'-end sensitively affects the target-binding activity. It is possible that the binding site of CPT1 is near the 3'-terminus guanine base ( $G^{36}$ ) that is incorporated into the G-quartet planar structure [26]. Therefore, in case of CA-17 and -18A that retained certain binding activities despite the presence of  $G^{37}$ ,  $G^{37}$  can participate in G-quartet formation instead of  $G^{36}$  if  $G^{34}$ , which is three nucleotide residues upstream of  $G^{37}$ , is shifted into a loop of the G-quadruplex.

However, if this is the case, it remains unknown why CA-70 and -40 that have long 3'-tails retain the binding activity. Before addressing this issue, we had to ascertain the differences between active and inactive fragments in the binding activity, because the abovementioned observations were made using fluorescence quenching titration; the degree of quenching is not necessary consistent with the target-binding ratio. Therefore, we analyzed CA-16 and -19 by the FP assay and confirmed that the former has evident CPT1-binding activity but the latter does not (Figure 4). Then, we speculated that the extra 3'-terminus  $G^{37}T^{38}A^{39}$  may interfere with G-quadruplex formation; however, CD spectra showed that both CA-16 and -19 formed a parallel G-quadruplex in either buffer solution [27,28] (Figure 5). Also, the  $K^+$  dependency on G-quadruplex formation was confirmed (Figure 4b). A similar G-core sequence ( $AG_3TG_4AG_3TG_4$ ) in a promoter region of c-Myc gene is known to form a three-tiered parallel G-quadruplex [29,30]. Therefore, it is conceivable that CAs can form parallel G-quadruplexes, although CAs have short loops consisting of 1–2 nucleotide residues. These parallel G-quadruplex cores are extremely stable. The  $T_m$  value of CA-16 was observed to be 73  $^\circ\text{C}$  in 10 mM PBS buffer (Figure 7). The  $T_m$  value was elevated by 80  $^\circ\text{C}$  when CPT1 associated with CA-16, indicating a significant contribution to the thermodynamic stability owing to  $\pi$ - $\pi$  stacking interaction between the G-quartet plane and heterocyclic rings of the target.

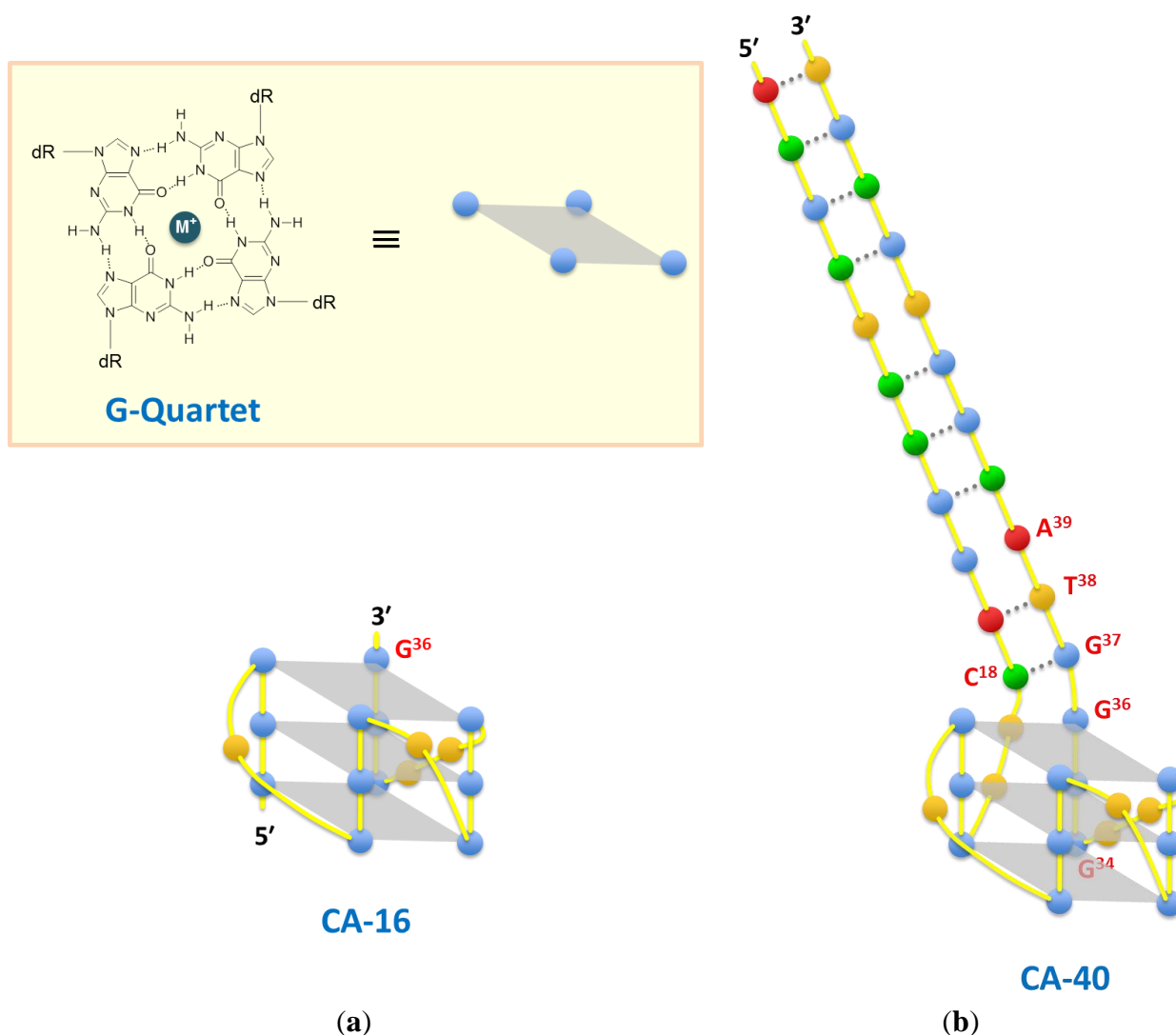
**Figure 7.** Melting curves for CA-16 in the presence (red) and absence (black) of CPT1, which were obtained by plotting the ellipticity at 265 nm against the temperature.



Overall, our experimental data indicated that the 3'-tail would not interfere with G-quadruplex formation but would interfere with target binding to the G-quartet plane involving  $G^{36}$ . The first base of the 3'-tail may compete with CPT1 against space for binding on the adjacent G-quartet plane. However, in case of CA-70 and -40, the first base of the 3'-tail  $G^{37}$  pairs with  $C^{18}$  and is involved in forming the stem duplex. This may provide conformational stress on the whole structure, resulting in a bend in the joint of the stem and G-quadruplex and consequently create room for target binding on the

G<sup>36</sup>-containing G-quartet plane (Figure 8b). To verify this hypothesis, we further generated two truncated fragments (CA-23A and -23B), having the G-core sequence with a 3'-tail of GTA and 5'-tail of ACTT or TTTT, and subsequently compared their binding activities. CA-23A can form two successive base pairs between both tails, whereas CA-23B cannot. As expected, CA-23A retained the binding activity, whereas CA-23B exhibited little or no binding activity (Table 1 and Figure 3). Thus, these data demonstrated the importance of C<sup>18</sup>-G<sup>37</sup> base pairing in the aptamer-target interaction.

**Figure 8.** (a) Hydrogen-bonding pattern in a G-quartet (upper), and cartoon of a 16-mer parallel G-quadruplex, CA-16 (lower). (b) Cartoon of a putative conformation of CA-40. Base colors: red = adenine, blue = guanine, green = cytosine, and orange = thymine.



The binding specificities of active fragments were analyzed using CPT1, CPT2, and CPT (Figure 1). Except for CA-18A, fragments preferred targets in the following order: CPT1 > CPT2 > CPT. This was consistent with the binding specificity of the mother aptamer, CA-70 (Table 1). These results were reasonable because CPT1 was used for SELEX to find CPT-binding DNA aptamers. Although, the specificity of binding of CA-70 was not as specific as that of CPT-binding modified DNA aptamers reported previously [13], CA-70 could clearly distinguish CPTs from other aromatic

compounds, such as 9(10*H*)-acridone, 2-(carboxymethyl)-9(10*H*)acridone, and fluorescein ( $K_d$  values of  $>10 \mu\text{M}$ ), while it exhibited lower affinity for FMN ( $K_d = 8.5 \mu\text{M}$ ). Thus, subtle distortions on the  $G^{36}$ -containing G-quartet plane in addition to electrostatic interactions and steric hindrance with base-, sugar-, and phosphate moieties adjacent to  $G^{36}$  could form the binding site and enable specific binding of small molecules.

#### 4. Conclusions

Unlike antibody, the G-quadruplex does not appear to form complex tiny cavities to fit small ligands with large structural variations. However, many compounds that can bind to the G-quadruplex have been reported and sequences with the G-quadruplex motif can discriminate between small molecules based on specificity to a certain extent. We believe that the insights derived from our results will provide clues for devising a more universal approach for small ligand recognition using G-quadruplex DNA. Small molecules that target the G-quadruplex of a particular gene can be rationally designed and used in future for artificial gene regulation for bioresearch, bioengineering, and chemotherapy.

#### Acknowledgments

This study was partly supported by a Grant for Industrial Technology Research from the New Energy and Industrial Technology Development Organization (NEDO) of Japan, and by a Grant-in-Aid for Scientific Research (C), No. 25350962, from the Japan Society for the Promotion of Science (JSPS). Y.K. is grateful for a Research Fellowship from the Japan Society for the Promotion of Science (JSPS) for Young Scientists.

#### Conflicts of Interest

The authors declare no conflict of interest.

#### References

1. Ellington, A.D.; Szostak, J.W. *In vitro* selection of RNA molecules that bind specific ligands. *Nature* **1990**, *346*, 818–822.
2. Tuerk, C.; Gold, L. Systematic evolution of ligands by exponential enrichment: RNA ligands to bacteriophage T4 DNA polymerase. *Science* **1990**, *249*, 505–510.
3. Ellington, A.D.; Szostak, J.W. Selection *in vitro* of single-stranded DNA molecules that fold into specific ligand-binding structures. *Nature* **1992**, *355*, 850–852.
4. Sissi, C.; Gatto, B.; Palumbo, M. The evolving world of protein-G-quadruplex recognition: a medicinal chemist's perspective. *Biochimie* **2011**, *93*, 1219–1230.
5. Hamon, F.; Faverie, A.; Renaud, F.A.; Hamon, F.; Di Primo, C.; Largy, E.; Dausse, E.; Delaurière, L.; Landras-Guetta, C.; Toulmé, J.J.; *et al.* Nucleic acids targeted to drugs: SELEX against a quadruplex ligand. *Biochimie* **2011**, *93*, 1357–1367.
6. Tucker, W.O.; Shum, K.T.; Tanner, J.A. G-quadruplex DNA aptamers and their ligands: Structure, function and application. *Curr. Pharm. Des.* **2012**, *18*, 2014–2026.

7. Nadai, M.; Sattin, G.; Palù, G.; Palumbo, M.; Richter, S.N. Clerocidin-mediated DNA footprinting discriminates among different G-quadruplex conformations and detects tetraplex folding in a duplex environment. *Biochim. Biophys. Acta* **2013**, *1830*, 4660–4668.
8. Gatto, B.; Palumbo, M.; Sissi, C. Nucleic acid aptamers based on the G-quadruplex structure: therapeutic and diagnostic potential. *Curr. Med. Chem.* **2009**, *16*, 1248–1265.
9. Smirnov, I.V.; Shafer, R.H. Electrostatics dominate quadruplex stability. *Biopolymers* **2007**, *85*, 91–101.
10. Nagatoishi, S.; Isono, N.; Tsumoto, K.; Sugimoto, N. Loop residues of thrombin-binding DNA aptamer impact G-quadruplex stability and thrombin binding. *Biochimie* **2011**, *93*, 1231–1238.
11. Nagatoishi, S.; Sugimoto, N. Interaction of water with the G-quadruplex loop contributes to the binding energy of G-quadruplex to protein. *Mol. Biosyst.* **2012**, *8*, 2766–2770.
12. Pramanik, S.; Nagatoishi, S.; Sugimoto, N. DNA tetraplex structure formation from human telomeric repeat motif (TTAGGG):(CCCTAA) in nanocavity water pools of reverse micelles. *Chem. Commun.* **2012**, *48*, 4815–4817.
13. Imaizumi, Y.; Kasahara, Y.; Fujita, H.; Kitadume, S.; Ozaki, H.; Endoh, T.; Kuwahara, M.; Sugimoto, N. Efficacy of base-modification on target binding of small molecule DNA aptamers. *J. Am. Chem. Soc.* **2013**, *135*, 9412–9419.
14. McLuckie, K.I.; Waller, Z.A.; Sanders, D.A.; Alves, D.; Rodriguez, R.; Dash, J.; McKenzie, G.J.; Venkitaraman, A.R.; Balasubramanian, S. G-quadruplex-binding benzo[a]phenoxazines down-regulate c-KIT expression in human gastric carcinoma cells. *J. Am. Chem. Soc.* **2011**, *133*, 2658–2663.
15. Hurley, L.H.; von Hoff, D.D.; Siddiqui-Jain, A.; Yang, D. Drug targeting of the c-MYC promoter to repress gene expression via a G-quadruplex silencer element. *Semin. Oncol.* **2006**, *33*, 498–512.
16. Shoji, A.; Hasegawa, T.; Kuwahara, M.; Ozaki, H.; Sawai, H. Chemico-enzymatic synthesis of a new fluorescent-labeled DNA by PCR with a thymidine nucleotide analogue bearing an acridone derivative. *Bioorg. Med. Chem. Lett.* **2007**, *17*, 776–779.
17. Beno, I.; Rosenthal, K.; Levitine, M.; Shaulov, L.; Haran, T.E. Sequence-dependent cooperative binding of p53 to DNA targets and its relationship to the structural properties of the DNA targets. *Nucleic Acids Res.* **2011**, *39*, 1919–1932.
18. Nagesh, N.; Sharma, V.K.; Ganesh, K.A.; Lewis, E.A. Effect of Ionic Strength on Porphyrin Drugs Interaction with Quadruplex DNA Formed by the Promoter Region of C-myc and Bcl2 Oncogenes. *J. Nucleic Acids* **2010**, *2010*, 146418.
19. Jecklin, M.C.; Schauer, S.; Dumelin, C.E.; Zenobi, R. Label-free determination of protein-ligand binding constants using mass spectrometry and validation using surface plasmon resonance and isothermal titration calorimetry. *J. Mol. Recognit.* **2009**, *22*, 319–329.
20. Ruta, J.; Perrier, S.; Ravelet, C.; Fize, J.; Peyrin, E. Noncompetitive fluorescence polarization aptamer-based assay for small molecule detection. *Anal. Chem.* **2009**, *81*, 7468–7473.
21. Mohanty, J.; Barooah, N.; Dhamodharan, V.; Harikrishna, S.; Pradeepkumar, P.I.; Bhasikuttan, A.C. Thioflavin T as an efficient inducer and selective fluorescent sensor for the human telomeric G-quadruplex DNA. *J. Am. Chem. Soc.* **2013**, *135*, 367–376.

22. Chen, S.B.; Shi, Q.X.; Peng, D.; Huang, S.Y.; Ou, T.M.; Li, D.; Tan, J.H.; Gu, L.Q.; Huang, Z.S. The role of positive charges on G-quadruplex binding small molecules: Learning from bisaryldiketene derivatives. *Biochim Biophys Acta* **2013**, *1830*, 5006–5013.
23. Shi, S.; Huang, H.L.; Gao, X.; Yao, J.L.; Lv, C.Y.; Zhao, J.; Sun, W.L.; Yao, T.M.; Ji, L.N. A comparative study of the interaction of two structurally analogous ruthenium complexes with human telomeric G-quadruplex DNA. *J. Inorg. Biochem.* **2013**, *121*, 19–27.
24. SantaLucia, J., Jr. A unified view of polymer, dumbbell, and oligonucleotide DNA nearest-neighbor thermodynamics. *Proc. Natl. Acad. Sci. USA* **1998**, *95*, 1460–1465.
25. Zuker, M. Mfold web server for nucleic acid folding and hybridization prediction. *Nucleic Acids Res.* **2003**, *31*, 3406–3415.
26. Sen, D.; Gilbert, W. Formation of parallel four-stranded complexes by guanine-rich motifs in DNA and its implications for meiosis. *Nature* **1988**, *334*, 364–366.
27. Giri, B.; Smaldino, P.J.; Thys, R.G.; Creacy, S.D.; Routh, E.D.; Hantgan, R.R.; Lattmann, S.; Nagamine, Y.; Akman, S.A. Vaughn, J.P. G4 resolvase 1 tightly binds and unwinds unimolecular G4-DNA. *Nucleic Acids Res.* **2011**, *39*, 7161–7178.
28. Kasahara, Y.; Irisawa, Y.; Fujita, H.; Yahara, A.; Ozaki, H.; Obika, S.; Kuwahara, M. Capillary electrophoresis-systematic evolution of ligands by exponential enrichment selection of base- and sugar-modified DNA aptamers: target binding dominated by 2'-O,4'-C-methylene-bridged/locked nucleic acid primer. *Anal. Chem.* **2013**, *85*, 4961–4967.
29. Seenisamy, J.; Rezler, E.M.; Powell, T.J.; Tye, D.; Gokhale, V.; Joshi, C.S. Siddiqui-Jain, A.; Hurley, L.H. The dynamic character of the G-quadruplex element in the c-MYC promoter and modification by TMPyP4. *J. Am. Chem. Soc.* **2004**, *126*, 8702–8709.
30. Kang, H.J.; Park, H.J. Novel molecular mechanism for actinomycin D activity as an oncogenic promoter G-quadruplex binder. *Biochemistry* **2009**, *48*, 7392–7398.

© 2013 by the authors; licensee MDPI, Basel, Switzerland. This article is an open access article distributed under the terms and conditions of the Creative Commons Attribution license (<http://creativecommons.org/licenses/by/3.0/>).